Geometric aspect of intergrain flux penetration and pinning in $YBa_2Cu_3O_7$ ceramics

M. A.-K. Mohamed* and J. Jung
Department of Physics, University of Alberta, Edmonton, Alberta, Canada T6G 2J1
(Received 13 August 1990; revised manuscript received 18 January 1991)

We report on studies of the magnetic properties of ceramic $YBa_2Cu_3O_{7-\delta}$ modified by the sample geometry (shape). The measurements of the diamagnetic shielding, the Meissner effect, the trapped field, and the relaxation phenomena were performed at 77 K and over a range of applied magnetic fields 0–1200 G for the sintered sample (whose shape was changed from a disk to a ring and finally to a broken ring) and for the pressed-powder disk-shaped sample. These studies allowed us to separate the intergranular magnetic properties of the ceramic sample from the intragranular ones. The studies revealed the effect of the macroscopic shielding currents, weak links, grain-decoupling process, and intergrain vortex-field gradients penetrating the sample on the shielding properties of the ceramic sample at low applied magnetic fields. The relaxation rate of the trapped intergrain flux depends on the sample geometry. An effective activation energy for the intergranular flux creep equal to 1.25 ± 0.3 eV at 77 K was found in the disk-shaped sintered sample. An effective activation energy for the intragranular flux creep equal to 0.05 ± 0.01 eV (the zero-field-cooled case) and 0.09 ± 0.02 eV (the field-cooled case) at 77 K was found in the pressed-powder disk-shaped sample of the same dimensions. We applied the critical-state model of Däumling and Larbalestier [Phys. Rev. B **40**, 9350 (1989)], who calculated diamagnetic shielding in disk-shaped conventional superconductors, to explain the dependence of the intergrain component of the diamagnetic shielding in the ceramic disk and rings on an applied magnetic field. Good agreement between this model and the experimental data was obtained for applied magnetic fields above 100 G corresponding to the full critical state in the 2-mm-thick ceramic disk and ring.

I. INTRODUCTION

A large number of reports on magnetic properties of high-temperature superconducting ceramics have developed the model of granular superconductors as an assembly of superconducting grains weakly coupled by Josephson junctions.[1–4] At low magnetic fields these ceramics behave like a Josephson medium, with magnetic vortices penetrating through weak links and trapped within the intergranular space only. The pinning of the intergrain vortices arises from the inhomogeneity of the intergrain junction coupling strengths.[3] At high magnetic fields two processes occur: the magnetic flux enters the grain in the form of Abrikosov vortices, and the effective grain coupling is suppressed by the magnetic field.

Regarding low-field properties, the weak links limit the magnitude of shielding or transport currents that can flow across a superconducting sample. The number of weak links and their coupling energies affect diamagnetic shielding properties of superconducting ceramics, including the distribution of the shielding currents. When a small external magnetic field is applied to the sample, the magnetic flux penetrates into it in a form of Josephson vortices. The penetration process depends on pinning forces and local vortex-field gradients. Parameters such as the magnitude of magnetic-field gradients and the demagnetization factors are directly related to a geometry (shape) of a superconducting sample. Changing the geometry of the sample should modify its low magnetic-field properties such as shielding, pinning, and related relaxation phenomena.

Geometric effects in $YBa_2Cu_3O_7$ ceramics were reported by Dersch and Blatter,[5] showing the dependence of macroscopic critical-current density on sample geometry. Shape effects were also seen by Senoussi *et al.*[6] in their studies of the magnetization of a series of $YBa_2Cu_3O_7$ hollow cylinders. They reported deviations from the linear behavior of the magnetization over the low applied-magnetic-field range up to about 50 G.

Studies of the role of sample geometry in flux motion processes require, however, that several experimental conditions be satisfied. Measurements have to be performed on the same sample in order to rule out a possible difference in the weak-link properties between samples. Changes in geometry have to be chosen properly in order to assure a maximum of information about geometry-related modifications of superconducting properties. These modifications should be reflected by the measurements of the local superconducting properties, e.g., the distributions of magnetic field across a sample, their dependence on an external applied magnetic field, and related relaxation measurement, and not by the measurement of the total magnetization of a sample only.

The measurements of diamagnetic shielding and trapped field across a sample allow one to determine whether the critical state is reached in a whole sample or in its portion only. The concept of the critical state was introduced by Bean.[7] For a superconducting $YBa_2Cu_3O_7$ ceramics in low magnetic fields up to about 1 kG, this state means that supercurrents (shielding or trapping currents) flow at the level of the intergrain (transport) critical current J_{CT}. The critical-state model has been used by Frankel[8] to reproduce magnetic-field profiles measured in a transverse field in a thin disk of NbTi su-

perconductor. Frankel's calculations have been extended by Däumling and Larbalestier[9] to disks with varying aspect ratio r_0/d (where r_0 is the radius and d the thickness of a disk). They have calculated the magnetic fields generated by a superconducting disk in a transverse field when the whole sample is in the critical state and found that the axial magnetic field shielded at the center of the disk depends on the thickness of the disk and not on its radius: $H_z = \text{const} J_c d$. The adaptation of the critical-state model to disk geometry provides a method to determine values of the critical current J_c from measurements of magnetic-field profiles above a disk or to predict the shielding and trapping of a disk if J_c is known.

In this paper we report an effect of sample geometry on superconducting properties of disks and rings of $YBa_2Cu_3O_7$ ceramics made out of the same sample. We decided to keep the external dimensions of a sample the same, starting with a disk-shaped sintered sample and changing its geometry into rings by drilling different size holes in its center. The measurements were performed using five different geometries: a sintered ceramic disk, two rings, a broken ring, and, finally, a pressed-powder disk formed after pulverizing the broken ring. The studies of the sintered and pressed-powder disks allowed us to separate the intergrain and intragrain properties of $YBa_2Cu_3O_7$ ceramics. The studies of two rings of different inner hole diameter and the broken ring allowed us to find the influence of vortex-field gradients and macroscopic persistent current on magnetic flux motion. We measured the distributions of the diamagnetic shielding, the Meissner field, the trapped magnetic flux across the sample, and their dependence on an applied magnetic field (over the range 0–1200 G) and time (time scale up to 10^4–10^5 sec). These measurements were done at 77 K. The results showed the nature of the diamagnetic shielding and its relaxation at low applied magnetic fields, the contribution of intergrain and intragrain shielding currents into it, and the contribution of Josephson and Abrikosov vortex fields and macroscopic persistent currents into the trapped field and its relaxation. We have applied the critical-state model of Däumling and Larbalestier[9] (who calculated diamagnetic shielding in disk-shaped conventional superconductors) to explain the dependence of the intergrain component of the diamagnetic shielding in the ceramic disk and ring on an applied magnetic field.

II. EXPERIMENTAL PROCEDURE

The experiments were done using a ceramic sample of $YBa_2Cu_3O_{7-\delta}$. The sample was prepared using a standard solid-state reaction method from the metal oxides Y_2O_3 (99.995% purity), CuO(99.999% purity), and $BaCO_3$ (99.995% purity). The powders were mixed, ground, formed into a pellet, and calcined at 905 °C for 24 h in air. After reaction, the pellet was regrounded, and a new pellet was formed under a pressure of 7300 bar and sintered in flowing O_2 for 7 h at 925 °C. The average grain size was found to be 4.5 μm using scanning electron microscopy (SEM). The superconducting transition temperature was determined by dc magnetization and resistance measurements versus temperature [Fig. 1; $T_c(R=O)=90.0$ K; $T_c(\text{magn.})=91.2$ K]. The intragrain critical-current density equal to 4.2×10^5 A/cm^2 at 77 K was determined from a high-field (5.5T) hysteresis loop measurement.

The measurements of the distribution of the diamagnetic shielding, the Meissner field, the trapped field, and their dependence on an applied magnetic field and time were made at 77 K with an axial cryogenic Hall probe (sensitivity ±30 mG), which was scanned along the diameter of the sample. The diameter of the sensitive part of the probe was equal to 0.6 mm. The Hall probe did not generate a magnetic field above the sensitivity level. We did not register any field at a level of 0.1 mG. The probe measured the component of the magnetic field perpendicular to a sample at a distance of about 1mm from it. The probe was connected to a gaussmeter and a computer-controlled system which allowed measurements of fast decays of a magnetic field. A solenoid was used to generate magnetic fields (0–1200 G) in the direction perpendicular to the sample.

Five different sample geometries were used in these studies. The measurements were first performed on a disk-shaped ceramic sample (16 mm diameter and 2.2 mm thickness). Then a 3-mm-diam hole was drilled in its center and the measurements were repeated. In the third

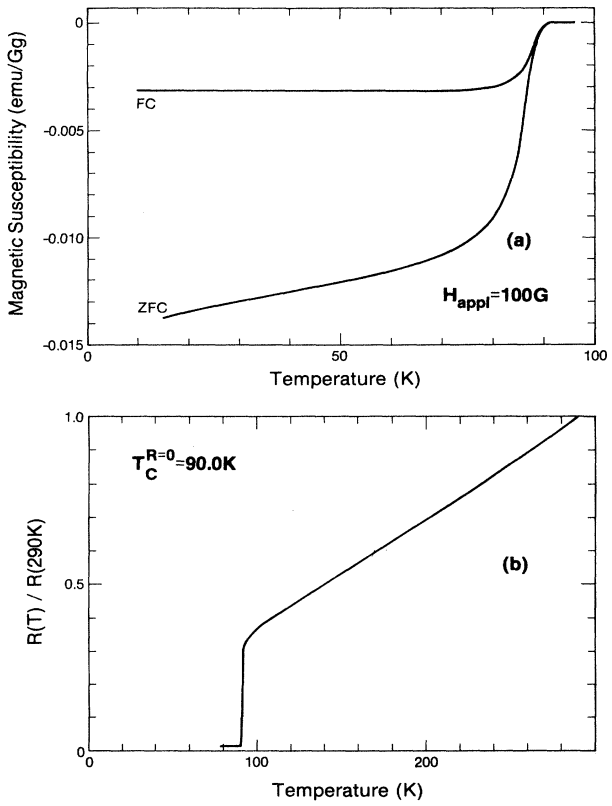

FIG. 1. (a) dc magnetization and (b) resistivity vs temperature of the ceramic sample of $YBa_2Cu_3O_{7-\delta}$ used in the experiments [$T_c(\text{magn.})=91.2$ K].

step this hole was enlarged to a diameter of 6 mm and the same experiments were performed. In order to avoid development of cracks, a hole was carefully drilled in a sealed sample using a tube-shaped diamond drill sprayed with water. Scanning electron microscopy did not reveal the presence of mechanical cracks at the resolution level of 0.1 μm. Finally, this ring was broken and the measurements were then repeated. In the fifth step the ring was pulverized (particle diameter 1–10 μm) and the powder obtained was pressed under a pressure of 7000 bar forming a disk of 16 mm outer diameter and 2.2 mm in thickness. This disk was not sintered in order to disable the weak-link effects. The measurements mentioned above were also done for this disk.

The measurements of transport critical-current density J_{CT} as a function of an applied magnetic field over a range of 20–1200 G were performed on zero-field-cooled sample at 77 K. J_{CT} was determined from the current-voltage curves measured using a dc four-probe technique. The voltage drop of 1 μV across the sample was used as the indication of reaching the critical-current value. These measurements were performed on a half-ring-shaped sample (of a cross-section area 1.0×2.2 mm^2) left after cutting a 6-mm-i.d. hole in a 3-mm-i.d. ring. The magnetic field was applied along the axis of this half-ring and in the direction perpendicular to the direction of the current.

III. EXPERIMENTAL RESULTS

We present the results of the measurements of the diamagnetic shielding, the Meissner field, the trapped field, and their dependence on an applied magnetic field, time, and a position across the superconducting sample of $YBa_2Cu_3O_{7-\delta}$. The measurements were performed for five different sample geometries: the sintered disk, the 3-mm-i.d. ring (ring No. 1), the 6-mm-i.d. ring (ring No. 2), the broken ring, and the pressed-powder disk. Both the zero-field-cooling (ZFC) and field-cooling (FC) measurements at 77 K were performed. The dependence of transport critical-current density on an applied magnetic field was measured for the ZFC case only.

A. Zero-field cooling

1. Spatial distribution of the diamagnetic shielding and the trapped field

The spatial distributions of shielding and trapped magnetic flux were measured at 77 K in all five samples, over an applied-magnetic-field range of 0–1200 G. Those distributions showed the penetration of the magnetic flux into the sample at low applied magnetic fields up to 50 G. For example, the spatial distributions, measured at applied fields between 19 and 20 G across the sample (Fig. 2), show the modifications of the diamagnetic shielding and the corresponding trapped magnetic field associated with the different geometry of the sample. In the sintered disk [Fig. 2(a)] the shielding is modified at the sample edges by the vortex-field gradients penetrating the sample. At low applied fields between 10 and 45 G, the magnetic flux is being trapped at the disk edges. Above 45 G the flux penetrates the whole disk and is trapped uniformity across the disk. In rings Nos. 1 and 2, the magnetic field is trapped inside the ring central holes, causing reduction of the shielding at their centers [Figs. 2(b) and 2(c)]. As a consequence, the macroscopic persistent current, circulating around the ring, is generated when the applied magnetic field is reduced to zero. It is important to note that only in the rings does the shielding decay with time. All the spatial field distributions measured over an applied field range 0–1200 G did not show measureable demagnetization effects at the sample edges.[10,11]

2. Diamagnetic shielding and the trapped field versus an applied magnetic field

The dependence of the diamagnetic shielding field on an applied magnetic field at 77 K is shown in Fig. 3 for all five geometries. (The shielding field is the difference between the applied magnetic field and the field measured by the Hall probe at the center of the disks and the rings and over the bulk of the broken ring.) The shielding of the sintered disk, measured at its center by the Hall probe, exhibits two maxima at applied fields of 35 and 150–200 G. Drilling a hole at the center of the disk reduces the first maximum and shifts it down to a lower applied field of around 19–20 G for ring No. 1 (3 mm i.d.) and further down to about 15–17 G for ring No. 2 (6 mm i.d.). This maximum is absent in the shielding of the broken ring and the pressed-powder disk. The second broad maximum at 150–200 G is independent of the external geometry of the sintered sample: disk, ring, or broken ring. However, if the sample is pulverized, this maximum disappears. The shielding of the pressed-powder disk reaches saturation above an applied field of 180 G. In the sintered samples the shielding saturates above 600 G and is essentially provided by the shielding currents flowing on the surface of the grains [Fig. 3(b)].

The dependence of the trapped magnetic field on an applied magnetic field at 77 K is presented in Fig. 4 for all five geometries. (The trapped field is the field measured by the probe at the center of the disks and the rings and over the bulk of the broken ring when the external applied field was reduced to zero.) The sintered disk starts to trap magnetic field at its edges starting at an applied field of 10 G. The trapped field saturates at applied fields above 500 G. The trapped field in the rings shows maxima: a broad one at an applied field of 150–200 G for both rings and a short one at a field of about 20–22 G in ring No. 2 (6 mm i.d.). If ring No. 2 is broken, the Hall probe does not reveal any magnetic field trapped in its center (within the accuracy of the measurement, ±30 mG). However, there is the field trapped in the bulk of the sample; its dependence on an applied field resembles that for the sintered disk. Finally, in the pressed-powder disk the field is trapped starting at an applied field of 100 G. The magnitude of the trapped field at 600 G is a factor of about 20 less than that measured in the sintered disk.

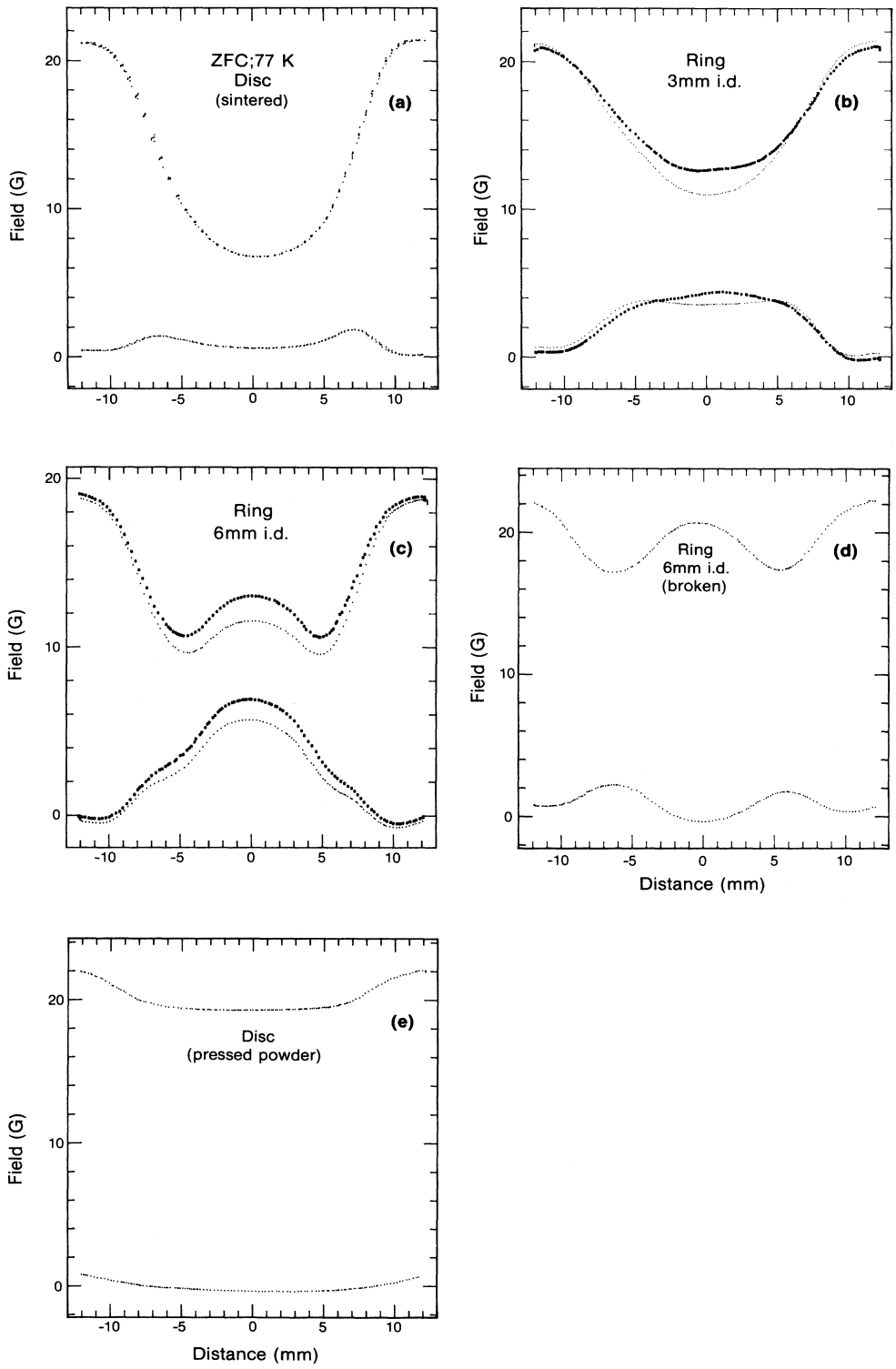

FIG. 2. Distributions of the diamagnetic shielding (the upper curves) measured across the sample at applied fields of 19–22 G and the trapped field (the lower curves) measured across the sample when the applied field was switched off. The dimensions +8 and −8 mm mark the sample outer edges. All measurements were done for the zero-field-cooled samples at 77 K. (a) The sintered disk; (b),(c) ring Nos. 1 and 2; the bold upper and lower curves show the diamagnetic shielding and corresponding trapped field measured after waiting 6×10^4 sec; (d) the broken ring; (e) the pressed-powder disk.

3. *Relaxation effects: The shielding and the trapped field*

Relaxations of both the shielding and trapped field were investigated at 77 K for all five sample geometries. All the decay rates measured over a time range between 1 and 10^4-10^5 sec are logarithmic in time. The measurements were done by the probe at the center of the disks and rings and over the bulk of the broken rings. The dependence of the relaxation rate of the diamagnetic shielding on an applied magnetic field can be observed only for the rings (Nos. 1 and 2) (Fig. 5) over a range of applied fields between 10 and 70 G. The decay rate of shielding in ring No. 1 reaches a maximum at an applied field of 19 G. The maximum decay rate in ring No. 2 occurs at a lower field of 16 G. The decay rates in ring No. 2 are about 2 times higher than in ring No. 1. The decay rates of shielding in the sintered disk, broken ring, and pressed-powder disk are applied-field independent, within the accuracy of our measurements.

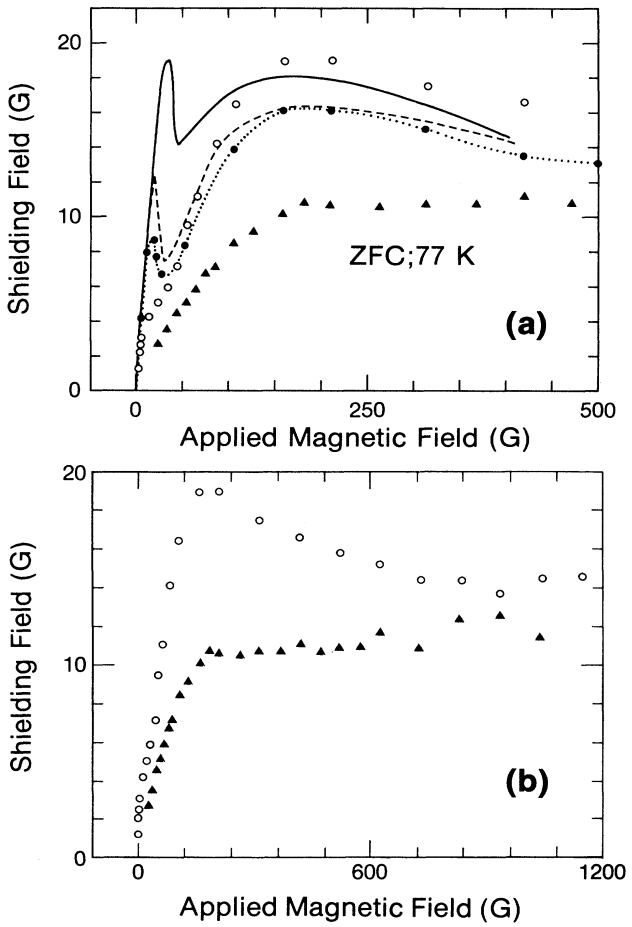

FIG. 3. Dependence of the diamagnetic shielding field on an applied field measured for all sample geometries at 77 K. Solid line, sintered disk; dashed line, ring No. 1 (3 mm i.d.); solid circles and dotted line, ring No. 2 (6 mm i.d.); open circles, broken ring; solid triangles, pressed-powder disk. Measurements were done by the probe over the bulk of the broken ring and in the center of all other samples.

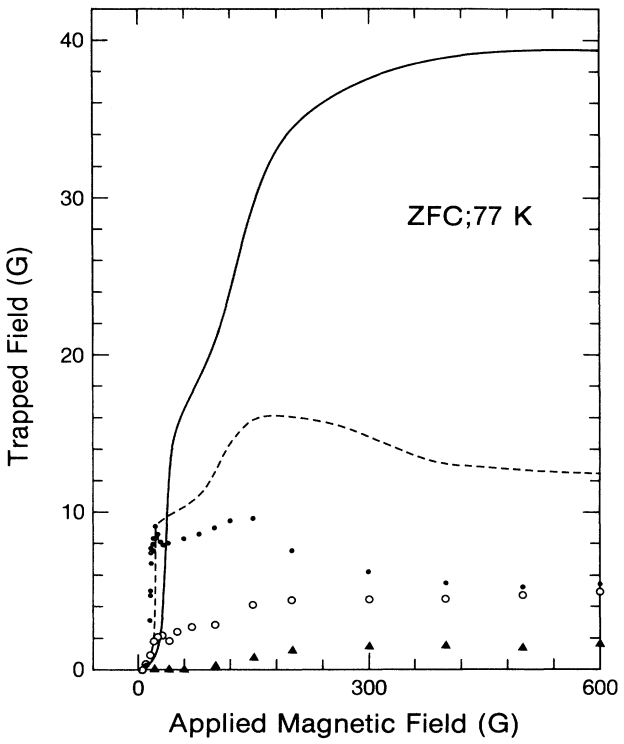

FIG. 4. Dependence of the field trapped in the zero-field-cooled samples at 77 K on an applied field. Solid line, sintered disk; dashed line, ring No. 1; solid circles, ring No. 2; open circles, broken ring; solid triangles, pressed-powder disk. The trapped field was measured by the probe over the bulk of the broken ring and in the center of the remaining samples.

The relaxation of the trapped field measured versus the initial trapped field for all five geometries is shown in Fig. 6. The decay rates of the trapped field increase if the

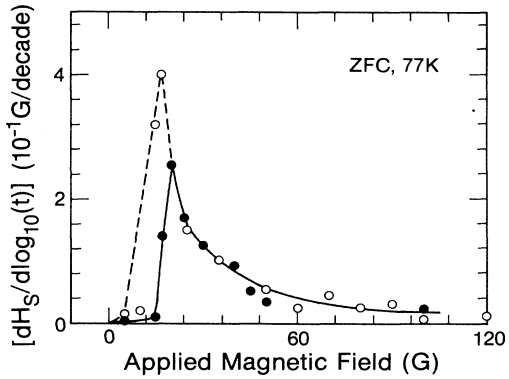

FIG. 5. Dependence of the logarithmic decay rate of the shielding on an applied field measured in the zero-field-cooled rings in their center at 77 K. Solid circles, ring No. 1; open circles, ring No. 2.

sample geometry changes from the disk to the ring. The same happens if ring No. 1 is transformed into ring No. 2. The measurement for the broken ring and pressed-powder disk reveals further increase in the decay rate. The decay rate is proportional to the initial trapped field for all geometries except for the rings. The rings show an anomalous behavior: The decay rate jumps to higher values at an initial trapped field of 9.5 G for ring No. 1 and 7.5 G for ring No. 2 (both the initial trapped fields correspond to an applied field of about 20 G) (Fig. 6).

4. *Dependence of transport critical-current density on an applied field*

The transport (intergrain) critical-current density J_{CT} was measured at 77 K over a range of applied fields between 20 and 1200 G. Figure 7 shows the decrease of J_{CT} from about 190 A/cm^2 for 20 G down to about 6–7 A/cm^2 for a 300–1200-G range. The measurement of J_{CT} was performed for the zero-field-cooled half-ring-shaped sample. The external magnetic field was applied in a direction perpendicular to the sample plane. This field orientation is similar to that used for the measurements of shielding and trapped flux in $YBa_2Cu_3O_{7-\delta}$ disks and rings.

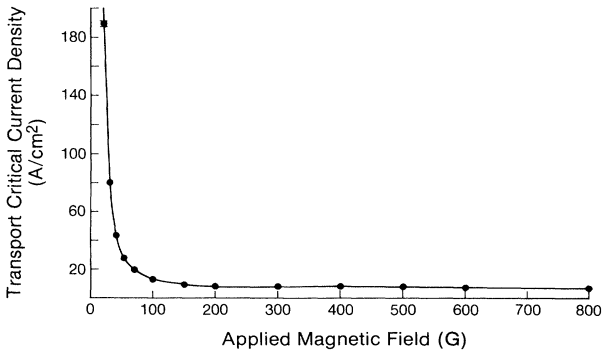

FIG. 7. Dependence of the transport critical-current density on an applied field at 77 K.

B. Field cooling

The measurements of the Meissner field, trapped field, and related relaxation phenomena were performed by the probe at the center of the disks and rings and over the bulk of the broken ring.

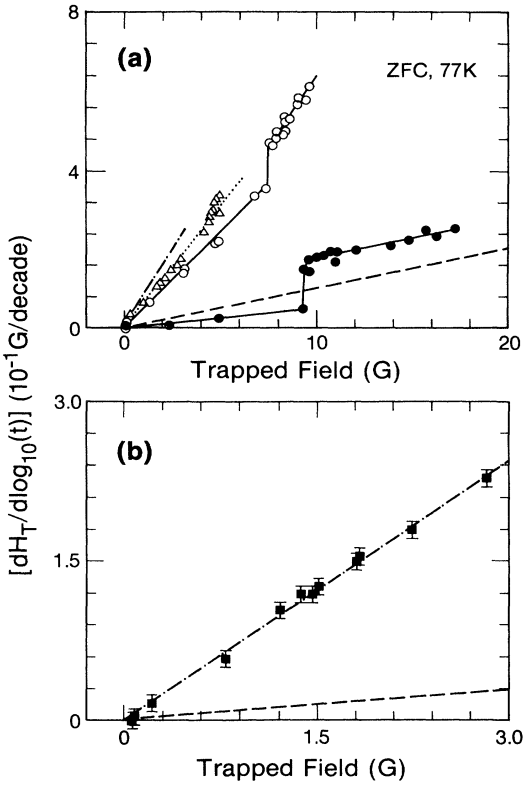

FIG. 6. Logarithmic decay rate of the field trapped in the zero-field-cooled samples at 77 K vs the initial trapped field. Dashed line, sintered disk; solid circles, ring No. 1; open circles, ring No. 2; open triangles, broken ring; solid squares and dot-dashed line, pressed-powder disk. The trapped field was measured by the probe over the bulk of the broken ring and in the center of the remaining samples.

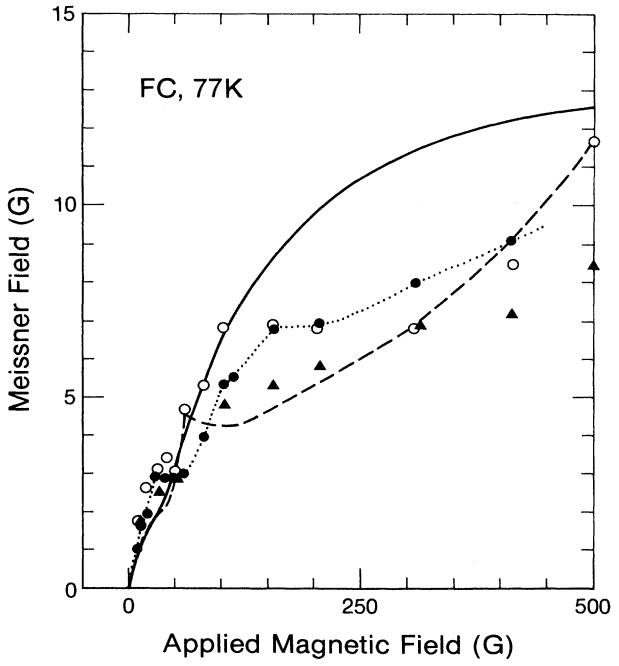

FIG. 8. Dependence of the Meissner field on an applied field measured in the field-cooled samples at 77 K. Solid line, the sintered disk; dashed line, ring No. 1; solid circles and dotted line, ring No. 2; open circles, broken ring; solid triangles, pressed-powder disk. The trapped field was measured by the probe over the bulk of the broken ring and in the center of the remaining samples.

1. *Meissner field and the trapped field versus an applied magnetic field*

The dependence of the Meissner field on an applied field is shown in Fig. 8 for all five geometries. The Meissner field of the rings and the broken ring was found to be reduced in comparison to that of the sintered disk above an applied field of 50–100 G. The Meissner effect of the pressed-powder disk is close to that observed in the rings.

The dependence of the trapped field on an applied field is shown in Fig. 9. The trapped field in the sintered disk reaches the saturation value above an applied field of 200 G. Rings Nos. 1 and 2 trap less flux; however, the trapped field exhibits a maximum at an applied field of 70 G in ring No. 1 and at a field of 50 G in ring No. 2. The flux trapping in the broken ring resembles that in the sintered disk. The magnitude of the field trapped in the pressed-powder disk at 600 G is a factor of about 13 smaller than that in the sintered disk.

2. *Relaxation effects: The Meissner field and the trapped field*

The relaxation effects of the Meissner field have been visible in ring No. 1 only. A time-dependent increase of the Meissner field was found over an applied-field range of 5–60 G. The logarithmic increase rate reaches a maximum of 0.4×10^{-1} G/decade at an applied field of 30–40 G.[10]

The dependence of the logarithmic decay rate of the trapped field on the initial trapped field is presented in Fig. 10. Changing the geometry of the sintered disk-shaped sample to the ring leads to an increase in the decay rate. The decay rate increases further if the measurements are done for the broken ring and subsequently for the pressed-powder disk.

IV. DISCUSSION

The most valuable information on the magnetic properties of $YBa_2Cu_3O_{7-\delta}$ ceramics at low magnetic fields has been provided by the zero-field-cooling experiments as the dependence of the diamagnetic shielding and trapped field on an applied magnetic field and the related

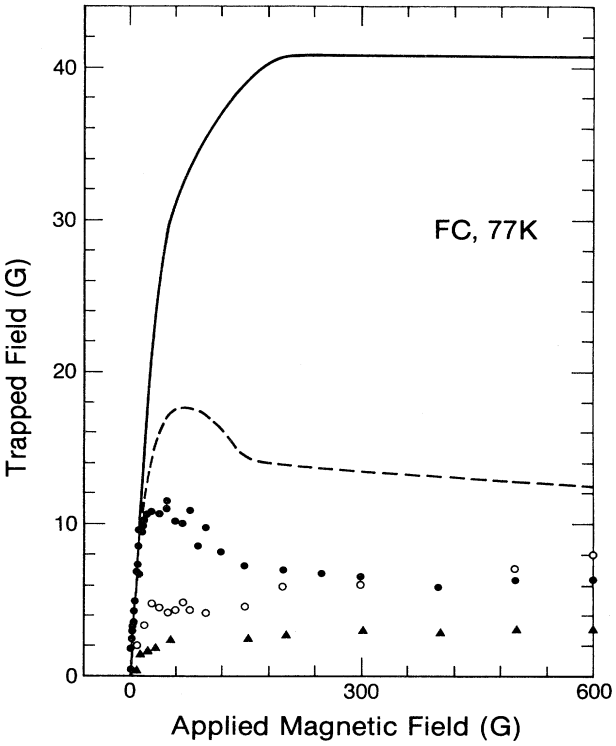

FIG. 9. The field trapped in the field-cooled samples at 77 K vs an applied field. Solid line, sintered disk; dashed line, ring No. 1; solid circles, ring No. 2; open circles, broken ring; solid triangles, pressed-powder disk. The trapped field was measured by the probe over the bulk of the broken ring and in the center of the remaining samples.

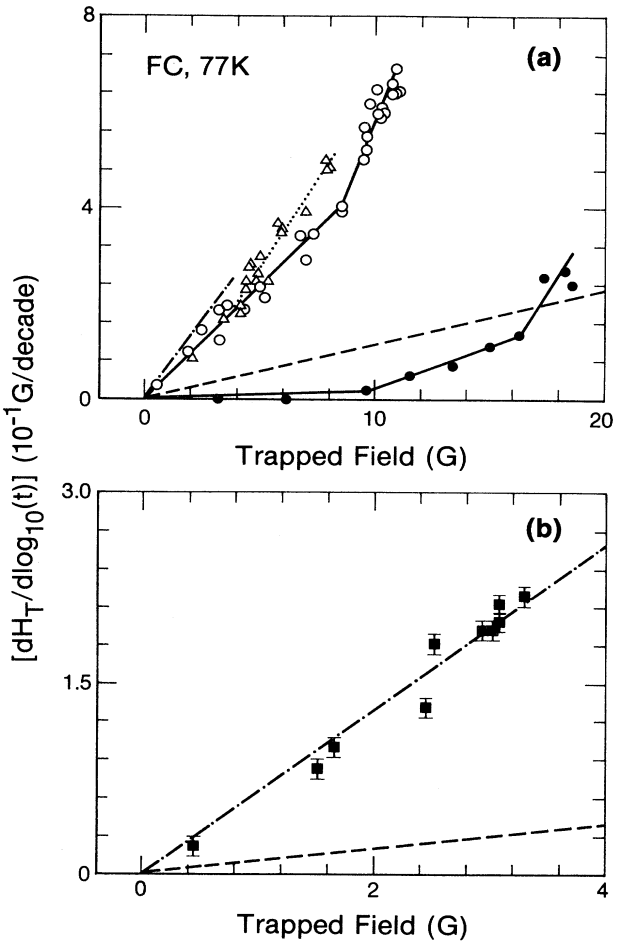

FIG. 10. Dependence of the logarithmic decay rate of the field trapped in the field-cooled samples at 77 K on the initial trapped field. Dashed line, sintered disk; solid circles, ring No. 1; open circles, ring No. 2; open triangles, broken ring; solid squares and dot-dashed line, pressed-powder disk. The trapped field was measured by the probe over the bulk of the broken ring and in the center of the remaining samples.

relaxation effects. Studies of the sintered and pressed-powder disks allowed us to distinguish between the intergranular and intragranular properties of $YBa_2Cu_3O_{7-\delta}$ ceramics, for example, to find the intergranular and intragranular components of the diamagnetic shielding. Studies of the rings allowed us to understand the following processes: the influence of the intergranular flux penetration and pinning on the diamagnetic shielding and the effect of the intergrain vortex-field gradients and macroscopic supercurrents on the effective activation energy for intergrain flux creep.

A. Nature of the diamagnetic shielding and the critical-state model

The intergrain component of the diamagnetic shielding can be seen (over an applied-field range of 0–600 G) as the difference between the diamagnetic shielding of the sintered disk and the pressed-powder disk (Fig. 3). The two maxima of the shielding field at 35 and 150–200 G are apparently associated with weak-link properties. The low-field peak magnitude depends on the sample geometry, whereas the second maximum is the geometry-independent feature. Measurement of the distributions of the shielding and trapped field across the zero-field-cooled sintered disk for different applied fields[11] helped us to understand the origin of the maximum of shielding at an applied field of 35 G. The decrease of shielding above 35 G could be attributed to the formation of large intergrain vortex-field gradients dB/dx penetrating the zero-field-cooled sample. These gradients are shown schematically in Fig. 11(a). The shielding currents are affected by the presence of intergrain weak links in $YBa_2Cu_3O_{7-\delta}$ ceramics which are believed to be Josephson tunnel junctions (S-I-S). The intergranular coupling energy is related to the intergrain critical current I_c by[3]

$$E_J = hI_c/2e \ , \tag{1}$$

and therefore limits the diamagnetic shielding currents in $YBa_2Cu_3O_{7-\delta}$ ceramics.

Because of the weakness of the intergranular coupling, the applied magnetic field penetrates deeply between grains, to the Josephson penetration depth λ_j along the grain boundaries. λ_j (using Clem's notation[2]) is expressible as

$$\lambda_j = (c\phi_0/8\pi^2 a_0 J_{CT}\mu_{\text{eff}})^{1/2} \ , \tag{2}$$

where $J_{CT} = I_c/a_0^2$ is the intergrain critical-current density, I_c is the maximum Josephson current, a_0 is the grain size, μ_{eff} is the permeability of granular material, and $\phi_0 = 2.07 \times 10^{-7}$ G cm^2 is the flux quantum. The corresponding Josephson lower critical field is equal to

$$H_{c1j} = (\phi_0/4\pi\lambda_j^2\mu_{\text{eff}})\ln(2\lambda_j/a_0) \ . \tag{3}$$

The transport-critical current density J_{CT}, measured over a range of applied magnetic fields between 20 and 1200 G at 77 K (Fig. 7), decreases from 189 A/cm^2 at 20 G down to 6.4 A/cm^2 at 1200 G. Taking the effective permeability[2] $\mu_{\text{eff}} = 0.3$ and the average grain size $a_0 = 4.5$ μm, we obtained $\lambda_j \simeq 3.2$, 8.5, 12.3, and 17.4 μm for an applied field of 20, 50, 100, and 1200 G, respectively. This gives a theoretical upper limit for H_{c1j} equal to about 0.1–0.2 G.

The experiments show that the zero-field-cooled ceramic disk of $YBa_2Cu_3O_{7-\delta}$ traps magnetic flux starting at an applied field of 10 G. On the other hand, the field-cooled sample starts to trap flux at applied magnetic fields below 1 G. Above H_{c1j} a type-II ceramic superconductor will show intergrain resistance and be unable to sustain a persistent current unless the pinning mechanism prevents the Lorentz force from moving the Josephson vortices. Two regimes have to be considered here: the Josephson vortex-flow regime and Josephson vortex-creep (pinning) regime. Those two processes apparently occur when the Josephson vortices penetrate the ceramic disk. The Josephson flux motion near the disk edges is a

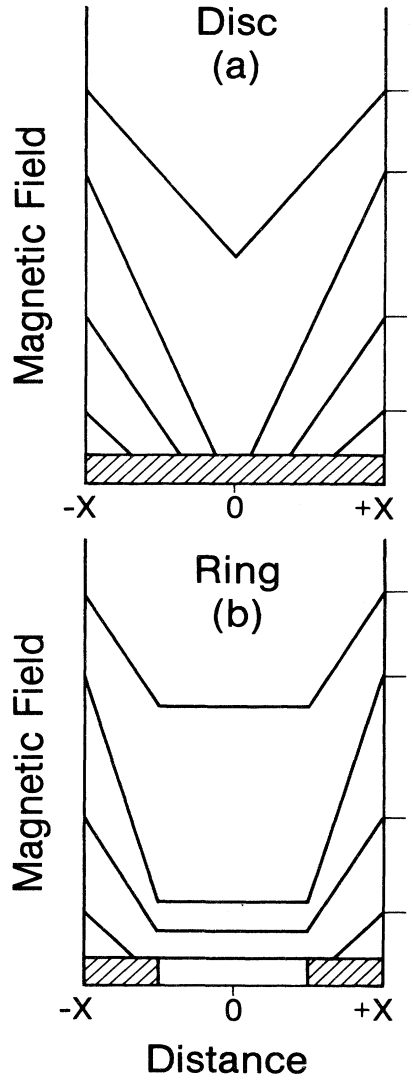

FIG. 11. Schematic picture of the vortex-field gradients penetrating (a) the zero-field-cooled disk and (b) the ring and modifying the diamagnetic shielding.

combination of a flow and creep of Josephson vortices. Evidence of this has been provided by the modification of the shielding field observed at low applied magnetic fields near the disk edges[11] and by the dependence of shielding on applied field [Fig. 3(a)].

The driving force acting on a single Josephson vortex of volume V in the presence of a Josephson vortex-field gradient dB_z/dr near the disk edge is[12]

$$F_r = \frac{B_z}{\mu_0}\frac{dB_z}{dr}V ,$$

where B_z is the local axial magnetic field perpendicular to the disk plane. This force is directed inward toward the center of the disk. If F_r is larger than the Josephson vortex-pinning force F_p, vortex flow leads to a partial destruction of persistent shielding currents at the disk edge. However, the Josephson vortex-field gradients dB_z/dr are reduced as one moves from the edge of the disk radially inward toward its center and the vortex flow is replaced by the vortex-creep process when F_r is smaller than F_p. The minimum of shielding observed at an applied field of about 45 G (Fig. 3) is apparently caused by the intergrain-vortex flow-induced dissipation mechanism. Above 45 G shielding starts to rise again. The distributions of the shielding and trapped field in the sintered disk[11] revealed that, starting at an applied field of 45 G, the magnetic flux is being trapped uniformly across the sample, suggesting the reduction of Josephson vortex-field gradients.

The magnitude of the maximum of shielding observed in the sintered disk at 35 G decreases if a hole is drilled in the center of the sintered disk. The reduction of this maximum depends on the hole size and is observed to be higher for ring No. 2 (6 mm hole i.d.) than for ring No. 3 (3 mm hole i.d.). In the rings, because of the central hole, the vortex-field gradients are larger than in the case of the sintered disk [Fig. 11(b)]. Therefore, the rate at which the intergranular vortices penetrate the ring is much larger than that for the disk. This interpretation is supported by the measurement of the logarithmic decay rate of shielding versus an applied magnetic field (Fig. 5). The decay rates of shielding in ring Nos. 1 and 2 show a maximum at applied magnetic fields of 19 and 16 G, respectively. At the same applied fields, the maxima of the shielding field are observed (Fig. 3). The magnitude of the decay rate of shielding measured at the maximum (Fig. 5) is higher in ring No. 2 than in ring No. 1. As a consequence, the shielding field of ring No. 2 measured over a range of applied fields, 15–20 G, is smaller than that of ring No. 1 (Fig. 3). This is consistent with the suggested picture of intergrain vortex-field gradients and vortex flow in the rings and the disk. The gradients in ring No. 2 are larger than those in ring No. 1. Studies of the diamagnetic shielding in the broken ring revealed the character of the shielding currents. The shielding of this sample consists of a single broad maximum at an applied field between 150–200 G (Fig. 3). The sharp maximum, visible in the sintered disk and rings over a range of applied fields, 15–35 G, is absent here. The shielding of the disk or the rings at low applied fields could be interpreted as due to macroscopic shielding current loops circulating around the sample. The interaction between the shielding current loops and vortex-field gradients leads to a minimum of shielding at an applied field between 35 and 45 G. Breaking the ring destroys those loops, and the role of shielding the external magnetic field is taken by small current loops, which provide, however, less effective shielding. The absence of the maximum of shielding between 15 and 35 G in the broken ring could therefore be associated with the missing macroscopic shielding current loops.

We believe that the reduction of the diamagnetic shielding observed in the rings over an applied field range of 15–70 G (Fig. 3) is not caused by demagnetization effects at the tips of cracks that could be produced during drilling a hole in the sintered disk. The way we prepared the rings ensures that drilling a hole into brittle $YBa_2Cu_3O_7$ does not introduce cracks. Careful examination of the ring material using SEM did not show any presence of mechanical cracks at the resolution level of 0.1 μm. Also, the distributions of the shielding field measured across ring No. 1 (Ref. 10) and ring No. 2 for applied fields over a range of 0–1000 G did not show any macroscopic enhancement of the internal magnetic field up to a value higher than an applied field. Note that, for example, at an applied field of 40 G, a field enhancement at least up to 50 G is required to suppress J_c and to explain the drop of the shielding of the ceramic disk of $YBa_2Cu_3O_{7-\delta}$ by 8–10 G (Fig. 13) when a hole is drilled in its center. On the other hand, the additional experimental evidence against crack-induced demagnetization effects could be obtained from the measurements of the magnetic properties of sintered disks of Fe-doped $YBa_2Cu_3O_{7-\delta}$ ($Y_1Ba_2Cu_{2.95}Fe_{0.05}O_{7-\delta}$) (Ref. 13) and $YBa_2Cu_3O_{7-\delta}$/intergrain Ag (<30 wt %) composite[14] (both disks have the same thickness as the $YBa_2Cu_3O_{7-\delta}$ ring). The first case concerns the dependence of the diamagnetic shielding on time (Fig. 5) that is observed for the rings of $YBa_2Cu_3O_{7-\delta}$ (but not for the sintered disk and the broken ring of $YBa_2Cu_3O_{7-\delta}$) over a range of applied fields between 10 and 70 G. This dependence could also be seen for the sintered disk of $YBa_2Cu_{2.95}Fe_{0.05}O_{7-\delta}$ over the same range of applied fields.[13] The second case deals with the reduction of shielding measured for the $YBa_2Cu_3O_{7-\delta}$ rings over an applied magnetic field range of 15–70 G, as compared to the magnitude of shielding at 150–200 G. The reduction of shielding over the same range of applied fields could also be found for the sintered disk of $YBa_2Cu_3O_{7-\delta}$/Ag (10 wt %) composite[14] (Fig. 12). The disks of $YBa_2Cu_{2.95}Fe_{0.05}O_{7-\delta}$ compound and $YBa_2Cu_3O_{7-\delta}$/Ag (10 wt %) composite were found by SEM to be internally crack free.[13,14] The ceramic sample of $YBa_2Cu_{2.95}Fe_{0.05}O_{7-\delta}$ contains voids and normal regions, and its magnetic properties resemble those of an assembly of many microscopic superconducting rings. In the $YBa_2Cu_3O_{7-\delta}$/Ag (10 wt %) composite, silver resides in the intergranular space of the ceramic sample, filling voids and coating $YBa_2Cu_3O_{7-\delta}$ grain boundaries. We believe that in both cases the presence of voids and normal regions increases the local intergrain vortex-field gra-

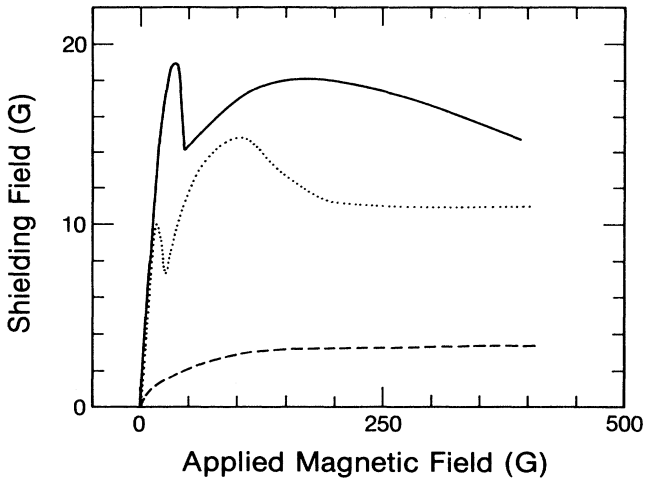

FIG. 12. Dependence of the diamagnetic shielding field measured in the zero-field-cooled samples at 77 K on an applied magnetic field. The measurement was done by the probe at the center of the disk-shaped samples (16 mm diameter and 2.2 mm thick). Solid line, pure ceramic $YBa_2Cu_3O_{7-\delta}$; dotted line, $YBa_2Cu_3O_{7-\delta}$/intergrain Ag (10 wt %) composite; dashed line, $YBa_2Cu_3O_{7-\delta}$/intergrain Ag (30 wt %) composite.

dients, and the reduction of shielding and its relaxation could therefore be explained by the strong interaction of intergranular vortices with macroscopic shielding currents. Note also that the dependence of the field trapped in the zero-field-cooled ring No. 2 on an applied field (Fig. 4) resembles that for the shielding field [Fig. 3(a)]. In both cases the field was measured at the center of the sample. The field trapping in the center of ring No. 2 is caused mainly by the macroscopic persistent current circulating around the ring. The first maximum at low applied field of 20 G is associated with the jump in the decay rate of the trapped field (Fig. 6) caused by the interaction of this current with intergranular vortices and not by demagnetization effects (e.g., at crack tips). The second maximum at 150 G is produced by partial grain-decoupling process.

The second maximum of shielding occurring at an applied field of 150–200 G does not depend on the shape of the sintered sample (Fig. 3). The applied field of 150–200 G could be related to a grain-decoupling field at which a high density of intergrain vortices drives a part of the intergrain junctions from the superconducting to the normal state. Note that the shielding of the sintered samples approaches that of the pressed-powder disk at applied fields above 600 G [Fig. 3(b)]. The shielding of the pressed-powder disk does not exhibit the two maxima mentioned above and saturates at applied fields above 180 G. The origin of this shielding appears to be an intragranular one. The weak links are destroyed in the pressed-powder disk, and the grains are shielded by the grain surface currents. The shielding saturates because of the penetration of Abrikosov-type vortices into the grains. It was observed (Fig. 4) that the pressed powder traps a flux starting at an applied field of 100 G, which is 10 times higher than the corresponding field for the flux trapping in the sintered disk-shaped sample. The measurement of the diamagnetic shielding versus an applied field, made on a disk-shaped sample of the $YBa_2Cu_3O_{7-\delta}$/intergrain silver composites[14] (Fig. 12), shows also the process of decoupling of the superconducting grains of $YBa_2Cu_3O_{7-\delta}$ separated by a layer of silver. The layer of silver causes complete grain decoupling in the $YBa_2Cu_3O_{7-\delta}$/Ag (30 wt %) composite when the thickness of the layer is larger than the normal metal coherence length $\xi_N \cong 20-70$ nm at 77 K.[15]

Frankel[8] measured and calculated profiles of the axial component of diamagnetic shielding across the thin disk of Nb-Ti/Cu composite material (46 mm diameter and 0.25 mm thickness). The critical-state model was adapted for this geometry and proved capable of reproducing the measured field profiles. The calculation of the field profiles was carried out with a model disk consisting of an array of coaxial current loops lying in the disk plane. The shielding field profiles in the Nb-Ti disk resemble those in the $YBa_2Cu_3O_{7-\delta}$ disk [Fig. 2(a)] except that demagnetization effects visible at the edges of the Nb-Ti disk are absent in the $YBa_2Cu_3O_{7-\delta}$ disk. The shielding field profiles generated in the Nb-Ti disk by applying an increasing field to the disk in which a magnetic field had been already trapped resemble those in the $YBa_2Cu_3O_{7-\delta}$ ring [Fig. 2(c)]. In this case the shielding of the ring could be reproduced by subtracting the fields generated by two disks: the disk filled with trapping currents $+J_c$ and the disk filled with shielding currents $-J_c$.

The magnetic fields occurring in disk-shaped conventional superconductors in the critical state in a transverse magnetic field have also been calculated by Däumling and Larbalestier[9] who extended the magnetic-field computations done by Frankel.[8] They found that the axial field shielded in the center of the disk is equal to const$\times J_c d$ (where d is the thickness of the disk) and does not depend on the disk radius r_0. The shielding currents also create radial fields which are of order $J_c d/2$ on the disk surface. In the disk center the radial field approaches zero. We have applied this model to explain the dependence of the axial component of shielding on an applied transverse magnetic field measured in the $YBa_2Cu_3O_{7-\delta}$ ceramic disk and ring at the center of the sample. Comparison of the axial shielding field $H_z = 2J_{CT}(H_{appl})d$ at the center of the sintered disk of $YBa_2Cu_3O_7$, calculated according to the model of Däumling and Larbalestier, with the experimental data on shielding of the ceramic disk and rings is shown in Fig. 13. Here $J_{CT}(H_{appl})$ was taken as the transport critical-current density measured for the ceramic $YBa_2Cu_3O_{7-\delta}$ as a function of applied field, and $d=2.2$ mm as the sample thickness. The shielding field of the sintered disk is marked with squares. However, the agreement with the model is better if one subtracts the shielding of the pressed-powder disk [Fig. 3(a)] from that of the sintered disk. The intergrain shielding of the disk obtained this way (Fig. 13, open circles) gradually decreases with increasing applied field, similarly to the

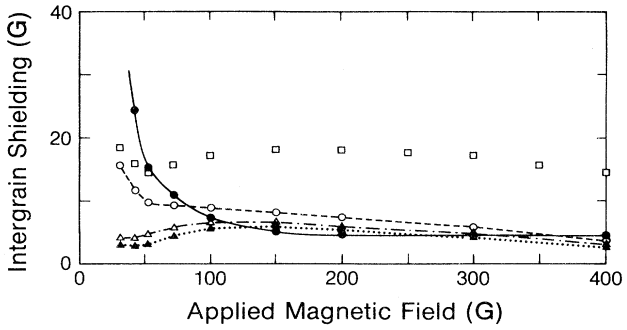

FIG. 13. Dependence of the intergrain diamagnetic shielding on an applied field at 77 K shown for the ceramic disk and rings. Full circles present theoretical results: the shielding of the disk calculated using the formula $H_z = 2J_{CT}d$ (Ref. 9); other symbols present experimental data. Open circles, the intergrain shielding of the disk obtained by subtracting the shielding of the pressed-powder disk [Fig. 3(a)] from that of the sintered disk (open squares). Open and solid triangles, the intergrain shielding of the ring Nos. 1 and 2, respectively.

dependence of J_{CT} on an applied field. Triangles show the intergrain shielding of two rings. One can see that the critical-state model of Däumling and Larbalestier applies to the $YBa_2Cu_3O_{7-\delta}$ ceramic disks (and rings) for an applied field above 70–100 G. At those fields the whole sample is in the critical state and the intergrain vortex-field gradients are reduced. At low applied fields, over the range between 0 and 70–100 G, only a portion of the sample is in the critical state (near to the outer edge) and the shielding currents are modified by the interaction with intergranular vortex-field gradients. The distributions of the field trapped in the sintered disk[11] reveal that the full penetration of the disk by intergrain vortices occurs at an applied field above 45–50 G.

B. Nature of the flux trapping

Comparison of the field trapped in the sintered disk-shaped sample with that trapped in the pressed-powder disk after zero-field cooling reveals that below an applied field of about 100 G the flux is trapped as intergranular Josephson vortices only (Fig. 4). Above this field intragranular vortices make an additional contribution to the trapped field, in fair agreement with the value of H_{c1} [$H_{c1}(\|c) = 200$ G, $H_{c1}(\perp c) = 50$ G at 77 K] measured in single crystals of $YBa_2Cu_3O_{7-\delta}$ by Krusin-Elbaum *et al.*[16] The contribution of both intergranular and intragranular vortices to the trapped field can still be observed at the maximum applied field of 1200 G.

In the ring one should expect three contributions to the trapped field: intergranular and intragranular vortices trapped in the bulk of the ring, and the magnetic flux, trapped inside the central hole, associated with the macroscopic persistent current circulating around the ring. The persistent current, similarly to the shielding currents, is sensitive to intergrain vortex-field gradients and the grain-decoupling process. The trapped field measured by the probe in the center of ring No. 2 as a function of an applied field turns out to be set up by the macroscopic persistent current. When ring No. 2 was broken, the probe did not measure any trapped field at the ring center. The sharp maximum observed at an applied field of 20–22 G (Fig. 4) is caused by the interaction of the persistent currents with a gradient of intergranular vortices. In consequence, this process is responsible for the Josephson vortex flow. This interpretation has been supported by the measurement of the trapped-field relaxation effects in the ring (Fig. 6), where a jump to a higher decay rate has been observed at a trapped field of 9.5 G (corresponding to an applied field of 20 G). The broad maximum at 150–200 G observed in both rings is associated with the partial grain-decoupling process as in the case of shielding (Fig. 3). Note the similarity between the shielding field and the trapped field measured versus an applied field in ring No. 2 (Figs. 3 and 4), suggesting a similar character of the macroscopic shielding currents and persistent trapping currents circulating around the ring.

The field trapped in the sintered sample or in the pressed-powder sample decays logarithmically in time (over the measured time scale from 1 up to 10^4–10^5 sec). The logarithmic decay rate of the trapped field is proportional to the initial trapped field for the sintered disk, pressed-powder disk, and broken ring (Fig. 6). The anomaly in the decay rates is observed for both ring Nos. 1 and 2. It exhibits a jump in the decay rate at the initial trapped fields of 9.5 and 7.5 G in the ring Nos. 1 and 2, respectively (both trapped fields correspond to an applied magnetic field of about 20 G). The most likely explanation of those jumps is the interaction of intergrain vortices with the macroscopic persistent currents. (Note that in the ring No. 2 the decay rate is that of the macroscopic persistent current. The interaction with vortices draws energy from the current and causes it to decay with the same rate as the trapped vortex field.) The other possibility could be the incomplete saturation of the trapped flux in low magnetic fields. The contour of the flux distribution measured across the rings at low fields look like two pyramids at the edges. Since half the flux relaxes inward, the relaxation rate is cut by half. When the flux becomes fully saturated at higher fields (a single pyramid), because of the contribution of the macroscopic persistent current, all flux relaxes outward, increasing the relaxation rate. However, when the persistent current contribution to the trapped field is gradually reduced because of a grain-decoupled process above an applied field of 150–200 G, the flux distribution contours again show two pyramids at the edges of the ring. The relaxation rates decrease gradually with the initial trapped field and do not exhibit a jump [Fig. 14(b)], ruling out the incomplete saturation of the trapped flux being responsible for the observed anomaly. This conclusion is also supported by the measurement of the decay rates of the flux trapped in the sintered disk. The flux distribution contours in the disk at low fields look like two pyramids at the disk edges [Fig. 2(a)], but no changes in the decay rates are found when the flux becomes saturated (Fig. 6).

The relaxation of magnetization has been analyzed by Anderson,[17] Kim and Stephen,[18] and Beasley, Labusch,

and Webb.[12] The dependence of the logarithmic decay rate $dM(t)/d\ln t$ on the initial magnetization $M(0)$ is given by

$$\frac{dM(t)}{d\ln t} = -M(0)\frac{kT}{E} , \tag{4}$$

where E is the activation energy for flux creep, k is the Boltzmann constant, and T is the temperature. This dependence was modified by Hagen, Griessen, and Salomons[19] and Griessen *et al.*[20] It has been shown that the dependence of the magnetization on time is given by the equation

$$M(t)=M(0)\left[1-\frac{kT}{E}\ln\left[1+\frac{t}{\tau}\right]\right] , \tag{5}$$

where τ is the relaxation time for flux motion. The relaxation time of magnetization calculated from this equation turns out to be

$$\frac{1}{M(t)}\frac{dM(t)}{d\ln t}\bigg|_{t=t_b} = -\left[\frac{E}{kT}-\ln\frac{t_b}{\tau}\right]^{-1} , \tag{6}$$

where t_b is the time at which the first magnetic relaxation data are recorded. Typical values of τ are 10^{-12}–10^{-6} sec,[20] and our experimental times t range from 1 to 10^4–10^5 sec for the ZFC case and from 10 to 10^4–10^5 sec for the FC case. An intermediate value of τ equal to 10^{-9} sec, $t_b=1$ sec for the ZFC case, and $t_b=10$ sec for the FC case have been used to calculate the activation energy for flux creep E in all investigated samples:

$$E=kT\left[-M(t)\Big/\frac{dM(t)}{d\ln t}\bigg|_{t=t_b}+\ln\left[\frac{t_b}{\tau}\right]\right] \tag{7a}$$

or

$$E=kT\left[-H_T(t)\Big/\frac{dH_T(t)}{d\ln t}\bigg|_{t=t_b}+\ln\left[\frac{t_b}{\tau}\right]\right] . \tag{7b}$$

The calculated values of the effective activation energy E are shown in Tables I and II. This energy represents the height of the energy barrier that has to be overcome by the moving vortex. If the vortex-field gradients or currents are present in the sample, an additional force F acts on the vortex and the energy barrier is being modified according to

$$E=E_{\text{eff}}=E_0\pm FVX , \tag{8}$$

where E_0 is the energy barrier in the absence of the vortex-field gradients or currents, V is the vortex volume, and X is the effective geometrical width of the energy barrier. E_{eff} can be either reduced or increased, depending on the sign of the vortex-field gradients.

The activation energy for flux creep in the sintered disk equal to 1.25±0.3 eV is close to that of 1.55 eV quoted by Maley *et al.*[21] for intergranular flux creep in a hollow cylinder of $YBa_2Cu_3O_{7-\delta}$ at 75 K and within a range of activation energies of 1–3 eV calculated by Murakami, Morita, and Koyama[22] for flux motion in $YBa_2Cu_3O_{7-\delta}$ ceramics at 1 kG and 77 K. On the other hand, the activation energy for flux creep in the pressed-powder disk equal to 0.052 ±0.010 eV (the ZFC case) and 0.085±0.020 eV (the FC case) should correspond to that quoted for single crystals of $YBa_2Cu_3O_{7-\delta}$. The activation energies in single crystals were found by Yeshurun *et al.*[23] from the dependence of magnetic relaxation $dM/d\ln t$ on an applied magnetic field (30 G to 30 kG) at 6 K. The values of E quoted are $E(\mathbf{H}\|\mathbf{c})=0.02$–$0.06$ eV

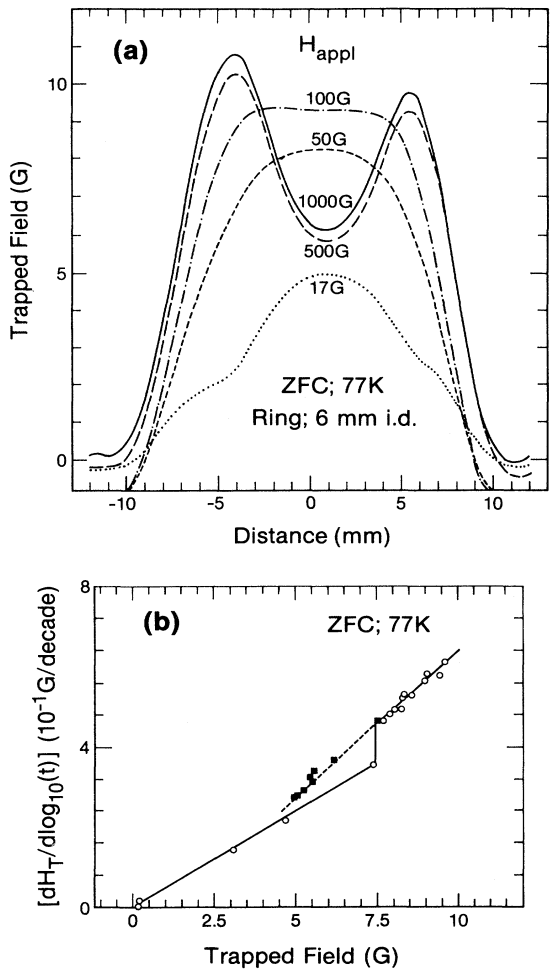

FIG. 14. (a) Contours of the flux trapped in the zero-field-cooled ring No. 2 at 77 K drawn for different applied fields. The grain-decoupling process above 150–200 G causes partial destruction of the persistent current and reduction of the flux in the middle of the ring. The asymmetry of the field trapped in the ring may be caused by a nonuniform microstructure of the sample (e.g., a nonuniform distribution of pinning centers, and Josephson junction coupling strengths). (b) Logarithmic decay rate of the field trapped in ring No. 2 vs the initial trapped field. Open circles, the decay rates corresponding to applied fields up to 150–200 G; solid squares, the decay rates corresponding to applied fields above 200 G; the decay rates gradually decrease with decreasing initial trapped field and increasing applied field from 200 up to 1200 G.

TABLE I. Activation energy E_{eff} for flux creep at 77 K (the ZFC case).

Sample geometry	E_{eff} (eV)	Range of the initial trapped field $H_T(t_b)$ (G)	Range of an applied field H_{appl} (G)	Flux motion process
Sintered disk	1.25±0.3	0–40	0–1200	creep
Ring No. 1	2.72±0.3	0–9.5	0–20	creep
(3 mm i.d.)	1.31±0.3	9.5–17	20–200	creep and flow
Ring No. 2	0.18±0.02	0–7.5	0–20	creep
(6 mm i.d.)	0.078±0.030	7.5–10	20–200	creep and flow
Broken ring No. 2	0.103±0.020	0–5	0–1200	creep
Pressed-powder disk	0.052±0.010	0–3	0–1200	creep

and $E(\mathbf{H}\perp\mathbf{c})=0.15$–$0.5$ eV. Hagen and Griessen[24] calculated the distribution of activation energies E^* for flux motion from the temperature dependence of the magnetic relaxation rate reported by Yeshurun and Malozemoff[25] for single crystals of $YBa_2Cu_3O_{7-\delta}$. $E_m^*=0.067$ eV, corresponding to the maximum of the distribution, was calculated.

In the rings the activation energy has been modified by the macroscopic persistent current circulating around the rings. The persistent current steepens the vortex-field gradients, reducing the activation energy [Eq. (6)] and creating a condition for flux flow.[10] At the initial trapped fields above 9.5 and 7.5 G (the applied fields above 20 G) in the zero-field-cooled ring Nos. 1 and 2, respectively, the flux motion is a combination of flux-creep and flux-flow-like processes (Fig. 6, Table I). Flux creep in the broken ring occurs at lower activation energy as compared with the sintered disk, suggesting that the vortex-field gradients are higher in the broken ring.

V. CONCLUSIONS

We investigated the modifications of the magnetic properties $YBa_2Cu_3O_{7-\delta}$ ceramics caused by the changes in the sample geometry. We also studied the difference in the magnetic properties of the sintered and pressed-powder disks. These studies allowed us to separate the intergranular properties of the ceramic sample from the intragranular ones. It was found that, at applied fields up to 600 G, the macroscopic shielding currents and weak links are responsible for the enhancement of the diamagnetic shielding of $YBa_2Cu_3O_{7-\delta}$ ceramics as compared to the shielding of $YBa_2Cu_3O_{7-\delta}$ powders. On the other hand, the interaction of the intergrain vortex-field gradients penetrating the sample with the macroscopic shielding currents leads to the vortex flow and the reduction of shielding at low applied fields of 15–45 G. In the rings this interaction becomes stronger because of the flow of intergrain vortices toward the central hole of the

TABLE II. Activation energy E_{eff} for flux creep at 77 K (the FC case).

Sample geometry	E_{eff} (eV)	Range of the initial trapped field $H_T(t_b)$ (G)	Range of an applied field H_{appl} (G)	Flux motion process
Sintered disk	1.25±0.3	0–40	0–1200	creep
Ring No. 1	10.5±5.0	0–10	0–20	creep
(3 mm i.d.)	0.72±0.10	10–16	20–40	creep
	~0.0–0.142	16–18	40–80	flow?
Ring No. 2	0.178±0.030	0–8.5	0–16	creep
(6 mm i.d.)	~0.0–0.013	8.5–11	16–50	flow?
Broken ring No. 2	0.180±0.030	0–4	0–20	creep
	0.056±0.020	4–8	20–1200	creep
Pressed-powder disk	0.085±0.020	0–3.5	0–1200	creep

ring. The grain-decoupling process is responsible for the further reduction of shielding above 150–200 G.

We applied the model of Daümling and Larbalestier[9] to simulate the dependence of the axial intergrain component of the shielding of the sintered ceramic disk and rings on an applied magnetic field. There is a good agreement between the result of this model ($H_z = 2J_c d$) and the measured intergrain shielding for applied fields above 70–100 G, at which the whole sample is in the critical state.

Regarding the trapped field and its relaxation rate, changing the geometry of the ceramic sample causes the activation energy to decrease from 1.25 down to about 0.1 eV. The Josephson vortex motion is a combination of the vortex flow and creep. In the rings the vortex flow is observed to be due to the interaction of the macroscopic persistent current with intergrain vortices. The field trapped in the pressed-powder disk decays with an activation energy between 0.052 ± 0.010 eV (the ZFC case) and 0.085 ± 0.020 eV (the FC case), which corresponds to that of 0.067 eV calculated for $YBa_2Cu_3O_{7-\delta}$ single crystals by Hagen and Griessen.[24]

ACKNOWLEDGMENTS

We thank A. P. Malozemoff and M. Däumling for useful discussions. This work was supported by grants from the Natural Sciences and Engineering Research Council of Canada (NSERC).

*Present address: Department of Physics, University of Lethbridge, Lethbridge, Alberta, Canada, T1K 3M4.

[1]A. P. Malozemoff, in *Physical Properties of High Temperature Superconductors,* edited by D. M. Ginsberg (World Scientific, Singapore, 1989).

[2]J. R. Clem, Physica C **153-155**, 50 (1988).

[3]M. Tinkham and C. J. Lobb, Solid State Phys. **42**, 91 (1989).

[4]D. P. Hampshire, X. Cai, J. Seuntjens, and D. C. Larbalestier, Supercond. Sci. Technol. **1**, 12 (1988).

[5]H. Dersch and G. Blatter, Phys. Rev. B **38**, 11 391 (1988).

[6]S. Senoussi, S. Hadjoudj, C. Weyl, and J. P. Fondere, Physica C **165**, 199 (1990).

[7]C. P. Bean, Phys. Rev. Lett. **8**, 250 (1962).

[8]D. J. Frankel, J. Appl. Phys. **50**, 5402 (1979).

[9]M. Däumling and D. C. Larbalestier, Phys. Rev. B **40**, 9350 (1989).

[10]M. A.-K. Mohamed, J. Jung, and J. P. Franck, Phys. Rev. B **41**, 6466 (1990).

[11]M. A.-K. Mohamed, J. Jung, and J. P. Franck, Phys. Rev. B **39**, 9614 (1989). (Note that the magnetic fields and decay rate quoted in this reference should be multiplied by a factor of 10.)

[12]M. R. Beasley, R. Labusch, and W. W. Webb, Phys. Rev. **181**, 682 (1969).

[13]M. A.-K. Mohamed, J. Jung, and J. P. Franck, Phys. Rev. B **41**, 4286 (1990).

[14]J. Jung, M. A.-K. Mohamed, S. C. Cheng, and J. P. Franck, Phys. Rev. B **42**, 6181 (1990).

[15]J. Moreland, R. H. Omo, J. A. Beall, and M. Madden, Appl. Phys. Lett. **54**, 1477 (1989).

[16]L. Krusin-Elbaum, A. P. Malozemoff, Y. Yeshurun, D. C. Cronemeyer, and F. Holtzberg, Phys. Rev. B **39**, 2936 (1989).

[17]P. W. Anderson, Phys. Rev. Lett. **9**, 309 (1962).

[18]Y. B. Kim and J. M. Stephen in *Superconductivity,* edited by R. D. Parks (Dekker, New York, 1969).

[19]C. W. Hagen, R. Griessen, and E. Salomons, Physica C **157**, 199 (1989).

[20]R. Griessen, C. F. J. Flipse, C. W. Hagen, J. Lensink, B. Dam, and G. Stollman, J. Less-Common Met. **151**, 39 (1989).

[21]M. P. Maley, M. E. McHenry, J. O. Willis, and M. McElfresh, Physica C **162-164**, 701 (1989).

[22]M. Murakami, M. Morita, and N. Koyama, Jpn. J. Appl. Phys. **28**, L1754 (1989).

[23]Y. Yeshurun, A. P. Malozemoff, F. Holtzberg, and T. R. Dinger, Phys. Rev. B **38**, 11 818 (1988).

[24]C. W. Hagen and R. Griessen, Phys. Rev. Lett. **62**, 2857 (1989).

[25]Y. Yeshurun and A. P. Malozemoff, Phys. Rev. Lett. **60**, 2202 (1988).